⌘ *Author's Choice*

THE JOURNAL OF BIOLOGICAL CHEMISTRY VOL. 284, NO. 6, pp. 3370–3378, February 6, 2009

Cell Entry of Arginine-rich Peptides Is Independent of Endocytosis*[S]

Received for publication, July 21, 2008, and in revised form, November 11, 2008 Published, JBC Papers in Press, December 1, 2008, DOI 10.1074/jbc.M805550200

Gohar Ter-Avetisyan[‡], Gisela Tünnemann[‡], Danny Nowak[‡], Matthias Nitschke[§], Andreas Herrmann[§], Marek Drab[¶], and M. Cristina Cardoso[‡‖1]

From the [‡]Max Delbrueck Center for Molecular Medicine, D-13125 Berlin, the [§]Department of Biology/Biophysics, Humboldt University Berlin, D-10115 Berlin, the [¶]Department of Molecular Biology, Max Planck Institute for Infection Biology, D-10117 Berlin, and the [‖]Department of Biology, Technische Universität Darmstadt, D-64287 Darmstadt, Germany

Arginine-rich peptides are a subclass of cell-penetrating peptides that are taken up by living cells and can be detected freely diffusing inside the cytoplasm and nucleoplasm. This phenomenon has been attributed to either an endocytic mode of uptake and a subsequent release from vesicles or to direct membrane penetration (transduction). To distinguish between both possibilities, we have blocked endocytic pathways suggested to be involved in uptake of cell-penetrating peptides. We have then monitored by confocal microscopy the uptake and distribution of the cell-penetrating transactivator of transcription (TAT) peptide into living mammalian cells over time. To prevent side effects of chemical inhibitors, we used genetically engineered cells as well as different temperature. We found that a knock-down of clathrin-mediated endocytosis and a knock-out of caveolin-mediated endocytosis did not affect the ability of TAT to enter cells. In addition, the TAT peptide showed the same intracellular distribution throughout the cytoplasm and nucleus as in control cells. Even incubation of cells at 4 °C did not abrogate TAT uptake nor change its intracellular distribution. We therefore conclude that this distribution results from TAT peptide that directly penetrated (transduced) the plasma membrane. The formation of nonselective pores is unlikely, because simultaneously added fluorophores were not taken up together with the TAT peptide. In summary, although the frequency and kinetics of TAT transduction varied between cell types, it was independent of endocytosis.

The discovery that the transactivator of transcription (TAT)[2] protein of human immunodeficiency virus type 1 was able to traverse cellular membranes and subsequently affected gene transcription (1, 2) led to the emergence of a new research field on cell-penetrating peptides (CPPs), also known as protein transduction domains (PTDs) or membrane transduction peptides (3). CPPs opened up the possibility to effectively deliver cell-impermeable hydrophilic compounds into living cells. The cargos reported to be shuttled to intracellular compartments include drugs (4), fluorophores (5), peptides (6–8), nucleic acids (9), proteins (10–12), nanoparticles (13), and liposomes (14, 15). The exact mechanism of cellular entry of CPPs remained unknown, but it was thought to be receptor-, energy-, and temperature-independent. In 2003 this unique mode of uptake was refuted as a methodological artifact, and endocytosis was suggested as the main pathway of cellular uptake of CPPs in live cells (16, 17). Arginine-rich peptides (RRPs) were not only historically the first (TAT) (1, 2) type of CPPs described, but they combined high uptake ability with moderate toxicity (18). Some groups observed a nonendocytic internalization pathway (8, 18–21), whereas others assigned CPP uptake to endocytic pathways, as CPPs were internalized and stored inside the vesicles. Endocytosis is broadly subdivided into phagocytosis and pinocytosis. Whereas phagocytosis is restricted to specialized cells like macrophages and leukocytes, pinocytosis occurs in all eukaryotic (or mammalian) cell types through at least four different endocytic pathways (22). Three of them have been implicated as routes for internalization depending on the CPP sequence and cargo of the CPPs as follows: clathrin-mediated endocytosis (23), caveolae-mediated endocytosis (24, 25), macropinocytosis (26–28), as well as the involvement of more than one endocytic pathway (16, 19). However, most of the studies so far utilized chemical inhibitors to characterize the contribution of a distinct endocytic pathway and could not exclude inhibitor-associated side effects.

RRPs such as TAT linked to high molecular weight cargos (*e.g.* proteins) were taken up into cells solely by endocytosis. When conjugated to low molecular weight cargos (*e.g.* peptides) however, in addition to be present in vesicles, they could be found freely diffusing in the cytoplasm and the nuclear compartment (8). However, a consensus regarding the latter uptake mode has not been reached. Our translocation studies of oligoarginines and oligolysines of various chain lengths and concentrations into living cells demonstrated the coexistence of two uptake modes (8, 18). Whereas a subset of the intracellular peptide was found inside cytoplasmic vesicles (Fig. 1*A*), some of the peptide displayed a rather homogeneous distribution

* This work was supported by grants from the Deutsche Forschungsgemeinschaft and the Volkswagen Foundation (to M. C. C.). The costs of publication of this article were defrayed in part by the payment of page charges. This article must therefore be hereby marked "*advertisement*" in accordance with 18 U.S.C. Section 1734 solely to indicate this fact.

⌘ *Author's Choice*—Final version full access.

[S] The on-line version of this article (available at http://www.jbc.org) contains supplemental Figs. S1–S5 and Movies 1–10.

[1] To whom correspondence should be addressed. Tel.: 49-6151-16-2377; Fax: 49-6151-16-2375; E-mail: Cardoso@bio.tu-darmstadt.de.

[2] The abbreviations used are: TAT, transactivator of transcription; BHK, baby hamster kidney; cav, caveolin; CHC, clathrin heavy chain; CPP, cell-penetrating peptide; DMEM, Dulbecco's modified Eagle's medium; FCS, fetal calf serum; FITC, fluorescein isothiocyanate; HIV, human immunodeficiency virus; KO, knockout; LMW, low molecular weight; PTD, protein transduction domain; RRP, arginine-rich peptide; TAMRA, 5,6-carboxytetramethylrhodamine; TAT-bt-SAv, TAT-biotin-streptavidin complex; tet, tetracycline; Tf, transferrin; tTA, transcriptional activator; WT, wild type.

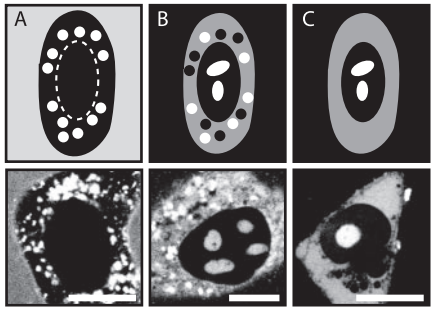

BHK-tTA/anti-CHC cells +tet	15 ± 2%	42 ± 2%	43 ± 3%
endothelioma cells (wt)	36 ± 3%	48 ± 2%	5 ± 3%
BHK21 cells	22 ± 5%	64 ± 3%	10 ± 2%
C2C12 cells	15 ± 3%	62 ± 2%	22 ± 2%

FIGURE 1. **Schematic illustration (*upper panel*), corresponding representative cell images, and relative proportions of the observed intracellular distributions of TAT CPP in different cell types after 1 h of incubation.** *A,* TAT peptide is present in the medium and in endocytic vesicles, but not freely available inside the cytoplasm or the nuclear compartment. *B,* TAT peptide reached all intracellular compartments and accumulated, in addition, in vesicles. *C,* TAT peptide is homogeneously distributed throughout the cytoplasm and accumulated in the nucleolus. *Scale bar,* 10 μm.

throughout the cytoplasm and high accumulation inside the nucleolar compartment (Fig. 1, *B* and *C*). The latter is henceforth termed transduction. It is still unclear whether transduction reflects CPPs that enter living cells by a not yet defined mechanism and/or CPPs that are released from endo- or lysosomes after endocytosis. To understand if both intracellular phenotypes are two distinct intermediate stages of the same process or indicate different uptake routes, we monitored the cytoplasmic and nucleolar localization of RRPs upon inhibition of endocytosis. In addition to TAT, we used the peptide PTD_4, which is an artificial, more amphipathic CPP with a reduced number of arginines and increased α-helical content compared with TAT (29). Most importantly, to suppress endocytic pathways, we restricted ourselves to the usage of genetically inducible systems, knock-out (KO) cell cultures, or physical methods, thus avoiding any potential side effects of chemical inhibitors of endocytosis.

EXPERIMENTAL PROCEDURES

Cells and Culture Conditions—The following cells were used: BHK21 (C-13) fibroblasts (baby hamster kidney clone 13, American Type Culture Collection), BHK21-tTA/anti-clathrin heavy chain (CHC) cell line (30), cav-1-KO and cav-1-wt mouse endothelioma cell lines (31), C2C12 mouse myoblasts (32), and 3T3 mouse fibroblasts (Invitrogen). The cells were cultured in Dulbecco's modified Eagle's medium (high glucose, with sodium pyruvate and L-glutamine) (PAA, Pasching, Austria) supplemented with 10 or 20% (the latter for C2C12 cells only) fetal calf serum (PAA, Pasching, Austria), 2 mM L-glutamine (Invitrogen), 50 μg/ml gentamicin (PAA, Pasching, Austria). For the cav-1-KO and cav-1 wild type (WT) endothelioma cell lines, the growth media was additionally supplemented with 1% nonessential amino acids (Sigma), 1% sodium pyruvate (Invitrogen), and 2 mM 2-mercaptoethanol diluted in phosphate-buffered saline (Invitrogen). For the BHK21-tTA/anti-CHC cell line, the following additives were added: 10% tetracycline-negative fetal calf serum (PAA, Pasching, Austria), 0.2 mg/ml geneticin (G418, Invitrogen), 0.5 μg/ml puromycin (Sigma), 2 μg/ml tetracycline (Sigma). For the induction of CHC antisense RNA expression, tetracycline was removed from the medium.

Peptides, Proteins, and Fluorophores—Peptides 5,6-carboxytetramethylrhodamine (TAMRA)-TAT (GRKKRRQRRR) and TAMRA-PTD_4 (YARAARQARA) (29) were synthesized as D-isomers and coupled directly to TAMRA at the N terminus (Peptide Specialty Laboratories GmbH, Heidelberg, Germany). Peptides and labels were diluted in RPMI 1640 medium without phenol red (PAA, Pasching, Austria) and applied at 10 μM final concentration to the cells. At lower concentrations, as we have shown previously (8), only the endocytic mode of uptake was detected (supplemental Fig. S1). To monitor CHC expression and function, transferrin (Tf) conjugated to Alexa Fluor 633 (Invitrogen) was added as a marker for clathrin-dependent endocytosis. Nonreactive forms of the fluorophores FITC (fluorescein isothiocyanate) and TAMRA were generated by incubation with Tris buffer (indicated by an asterisk) and used as a small molecule to monitor the generation of pores during the transduction event. To control for the complete inhibition of endocytosis at 4 °C, the globular protein TAT-biotin-streptavidin (TAT-bt-SAv) labeled with the fluorophore cyanine dye was used as an additional marker for fluid-phase uptake (supplemental Fig. S2).

Live Cell Uptake Experiments—For all experiments either 8-well μ-slides or 35-mm μ-dishes (Ibidi, Martinsried, Germany) were used. The cells were seeded onto the observation chambers and incubated overnight at 37 °C with 5% CO_2. The peptides TAMRA-TAT and TAMRA-PTD_4 (10 μM), the fluorophores FITC* and TAMRA* (10 μM), and Tf (10 μg/ml) were diluted in RPMI 1640 medium (PAA, Pasching, Austria) without phenol red and used at the indicated concentrations. Special care was taken to ensure that the volume of the peptide solution above the cells was comparable in the two different observation chambers and that the exchange against the appropriate peptide (label, marker) dilutions was performed very gently. Immediately after addition of the peptide (label, marker) to the cells, time lapses over 60 min (with time intervals of one image per min) were recorded. The experimental settings for the confocal microscope were identical for all experiments.

For the uptake experiments at 4 °C a custom-built cooling chamber was used. The height of this cooling chamber occupying the cooling flow and the radius of the loophole at the bottom were optimized to guarantee a constant temperature exchange between the 35-mm μ-dish observation chamber and the cool water flux. The temperature was regulated by a thermostat, and the exact temperature of 4 °C inside the medium above the cells was verified by measurements with a thermometer before and after the 1-h time lapses.

Microscopy, Image Acquisition, and Analysis—Confocal optical sections were acquired with a Zeiss confocal laser scanning microscope, LSM510 Meta, mounted on an Axiovert 200 M inverted microscope equipped with a live cell microscope incubation cage (Okolab, Ottaviano, Italy) using a 63× plan-apochromat NA1.4 oil immersion, phase-contrast objective.

The microscope incubation cage maintained a humidified atmosphere of 5% CO_2 and 37 °C, which was used throughout except for the low temperature experiments. For all settings the main beam splitter was HFT UV/488/543/633, and the specific parameters for the single fluorophores were as follows: FITC excited at 488 nm, detected with a 500–530-nm bandpass filter; TAMRA-TAT and TAMRA-fluorophore excited at 543 nm, detected with a 565–615-nm bandpass filter, transferrin-Alexa Fluor 633 excited with 633 nm, detected with a 650-nm long pass filter. Phase contrast images were recorded with excitation at 488 nm and detection in the transmission channel. The laser power for observation was 1% (488 nm, 25 milliwatts), 7% (543 nm, 1 milliwatt), and 25% (633 nm, 5 milliwatts). Settings were adjusted in a way that image pixels were not over- or underexposed with the range indicator function in the Zeiss laser scanning microscopy software version 3.2. To ensure that weak intracellular fluorescence signals of the peptides were not missed, a set of overexposed images was additionally collected.

For the quantification of transduction, 100–150 cells per transduction experiment were evaluated to obtain the percentage of transduced cells (indicated by nucleolar appearance of the labeled peptide), and the kinetics of TAT transduction was further characterized by the earliest time point when transduction could be detected within a field of view (initiation time of transduction).

Western Blotting—For Western blot analysis of the cav-1-KO and WT cells, half a million cells were counted, resuspended in 100 μl of phosphate-buffered saline, and boiled in Laemmli sample buffer for 10 min, and cell lysates were analyzed by SDS-PAGE followed by blotting onto polyvinylidene difluoride membranes. Signals were detected with the following primary antibodies: rabbit anti-Cav-1 polyclonal antibody (LifeSpan BioSciences, Inc., Seattle, WA) and mouse anti-Cav-2 and anti-Cav-3 monoclonal antibodies (1:2000 dilution, BD Transduction Laboratories). Anti-rabbit IgG-HRP (Sigma) and anti-mouse IgG-HRP (enhanced chemiluminescence, Amersham Biosciences) were used as secondary antibodies. Immunoreactive signals were visualized using enhanced chemiluminescence plus detection solution (Amersham Biosciences) and recorded using a luminescence imager (Luminescent Image Analyzer LAS-1000, FUJI Photo Film, Tokyo, Japan).

RESULTS

Because of their particularly high transduction ability, which solely depends on a minimal number of arginines, RRPs play a special role among CPPs (18, 33–35). To clarify the role of endocytosis in the uptake mode of CPPs with low molecular weight (LMW) cargos into living cells, we investigated the occurrence and extent of transduction of TAT and PTD_4 as CPPs with high and low transduction frequency, respectively (8). The intracellular distribution of peptides in living cells was analyzed by laser scanning confocal microscopy. To unravel the relevance of endocytic routes for the uptake and intracellular distribution of peptides, endocytic pathways were specifically inhibited by genetic approaches or were blocked in ensemble by incubation of cells at low temperature.

Role of Clathrin-mediated Endocytosis in CPP Uptake—Clathrin-dependent endocytosis represents a major endocytic pathway. For example, transferrin is taken up exclusively by this route, and several enveloped viruses (36), such as equine arteritis virus (37), exploit this route (38). As an early step of this route, upon binding of an extracellular ligand to specific cell-surface receptors, clathrin together with other adapter proteins builds an endocytic coat at the plasma membrane (Fig. 2*A*). The coated membrane buds and pinches off to form a cargo-filled vesicle (Fig. 2*A*).

Clathrin-dependent endocytic uptake of TAT has been repeatedly reported as a possible mechanism for CPP entry (23, 39, 40). To clarify the contribution of clathrin-dependent endocytosis in the uptake mode of arginine-rich CPPs, we used the BHK21-tTA/anti-CHC (30) cell line. This cell line expresses antisense CHC RNA under the control of a tetracycline-responsive element (Fig. 2*B*). More specifically, the transcription activator (tTA) is composed of the DNA binding domain of tetracycline repressor protein and a C-terminal activation domain of VP16 (herpes simplex virus protein) that functions as a strong transcription activator (41). The presence of tetracycline prevents binding of the transactivator tTA to the operator sequence and thus transcription of antisense RNA. In the absence of tetracycline the transactivator tTA binds to its operator sequence and activates the transcription of antisense RNA. As a consequence, the synthesis and functionality of CHC protein is significantly reduced, thereby suppressing clathrin-dependent endocytosis (30). The absence of tetracycline for 2 days was reported to inhibit 90% of transferrin internalization, and the expression of the CHC protein was reduced to 10% over 6 days in the absence of tetracycline (30). Therefore, to explore to what extent transduction of TAT depends on clathrin-dependent endocytosis, uptake of TAMRA-tagged TAT and PTD_4 was investigated in the presence (+tet) and absence (−tet) of tetracycline over 6 days. To simultaneously control the level of clathrin-dependent endocytosis, internalization of Alexa Fluor 633-labeled transferrin was monitored (Fig. 2*C*).

The control cells (+tet cells) are shown on the *left panel* of Fig. 2*C* and supplemental Fig. S3. TAT was homogeneously distributed throughout the cytoplasm and accumulated in the nucleolus (Fig. 2*C, arrowheads*) and therefore displayed the uptake mode of transduction. In addition, the labeled peptide was also present in cytoplasmic vesicles.

PTD_4 applied at the same concentration and monitored at identical confocal microscope settings did not show any transduction-associated cytoplasmic localization comparable with TAT. However, we observed the presence of PTD_4-containing vesicles (Fig. 2*C, left side, lower panel*). Fluorescent transferrin was internalized at high rates and enriched in the trans-Golgi network (42).

Inhibition of the clathrin-dependent endocytic pathway in −tet cells (Fig. 2*C* and supplemental Fig. S3*A*, *right panel*) was verified by the suppression of uptake of transferrin. TAT displayed the same intracellular distribution regarding the vesicular uptake as well as transduction, indicated by similar intensities inside the nucleolar compartment compared with the control (+tet) cells (Fig. 2*C* and supplemental Fig. S3). Similar to the control cells, no diffuse intracellular occurrence was observed for PTD_4, but in contrast to +tet cells the vesicular internalization of PTD_4 was almost completely abolished.

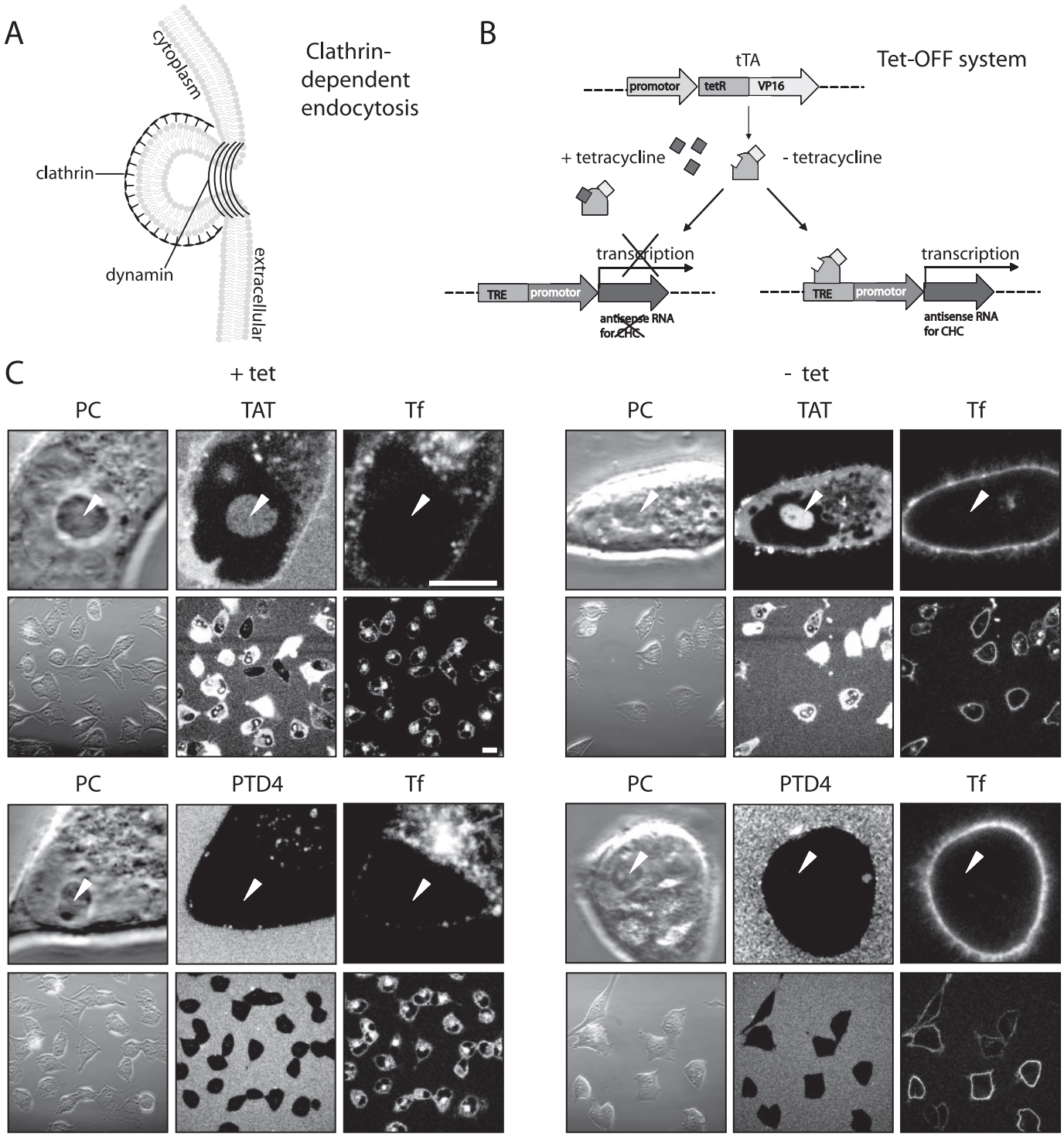

FIGURE 2. **Transduction of TAT is independent of clathrin-mediated endocytosis.** *A,* schematic diagram illustrating clathrin-dependent endocytosis. The clathrin coat is required for membrane invagination, and for the scission of clathrin-coated vesicles dynamin is needed. *B,* schematic representation of the Tet-Off system, allowing a conditional knockdown of CHC in the BHK21-tTA/anti-CHC cell line. The binding of the transcriptional activator tTA to an operator sequence in the absence of tetracycline (−*tet*) results in activation of transcription of CHC-antisense RNA and thereby repression of the CHC mRNA translation. *C,* confocal optical sections of living cells during incubation with the fluorescent CPPs TAT (*upper panel*) or PTD_4 (*bottom panel*) in the presence of the transferrin (*Tf*) as a marker for clathrin-dependent endocytosis. Each panel displays high magnification images of the phase contrast (*PC*) and the fluorescently labeled compound to show the details of their intracellular distribution and low magnification images to highlight the frequency of CPP transduction and Tf internalization (see also supplemental Fig. S3). *Arrowheads* mark the position of nucleoli. Transduction experiments were performed in the presence (*left panel*) and absence (*right panel*) of tetracycline. Although uptake of Tf is nearly abolished after tetracycline removal over a period of 6 days, the TAT CPP is still capable of reaching all intracellular compartments (diffuse, nonvesicular fluorescence, and accumulation inside nucleoli), indicating that this mode of uptake is not influenced by clathrin-dependent endocytosis. Vesicular uptake of the CPP TAT was still detected under −tet conditions albeit at reduced levels. *Scale bar,* 10 μm for high and 20 μm for low magnification images.

TAT Transduction Occurs in the Absence of Endocytosis

We confirmed that TAT transduction was observed in most cells by acquiring low magnification images (Fig. 2*C* and supplemental Fig. S3). To control for any potential side effects of tetracycline, the parental BHK21 cells (43, 44) were incubated with the CPPs and transferrin in the presence and absence of tetracycline. However, no difference of peptide transduction and vesicle formation was observed (data not shown). Therefore, we conclude that clathrin-dependent endocytosis is not required for transduction of the RRP TAT fused to an LMW cargo.

Role of Caveolin-mediated Endocytosis in CPP Uptake—Besides the classical clathrin-mediated endocytic pathway, caveolae-mediated endocytosis is one of the main endocytic entry routes into living cells (22, 45). For example, it is exploited by bacterial toxins and by simian virus 40 (36). Caveolae are flask-shaped, small (50–70 nm diameter) invaginations in the plasma membrane (Fig. 3*A*) that constitute membrane domains enriched in cholesterol and sphingolipids, called lipid rafts (46). Caveolae are characterized by the presence of the integral membrane protein caveolin-1 and are involved in the intracellular transport of lipid raft-associated molecules (47). This pathway has been repeatedly reported as an uptake route for CPPs into the cells (24, 25). Former studies used fluorescently labeled β-subunit of cholera toxin as a marker to monitor caveolar uptake. However, the pathway chosen by cholera toxin subunit β depends on the cell type (48) and hence may not be a faithful indicator for a single internalization pathway. To specifically inhibit only the caveolin-dependent route and to prevent the potential side effects caused by chemical inhibitors of endocytosis, we made use of an endothelial heart cell line generated from a knock-out (KO) mouse deficient for caveolin (cav-1) and the respective wild type (WT) cell line. As reported previously (31), in the absence of caveolin-1, caveolin-2 protein is degraded. This was corroborated by Western blot analysis (Fig. 3*B*). In contrast to WT cells, no cav-1 and cav-2 were detected in the KO cells, and in addition, antibodies directed against muscle cell-specific cav-3 gave a much weaker signal in the extract of KO cells compared with those from wild type cells.

To elucidate if caveolae-dependent endocytosis plays a role in the uptake mode of TAT with the LMW TAMRA, we applied TAT (Fig. 3*C*, *upper panel*, and supplemental Fig. S4) and PTD_4 (Fig. 3*C*, *middle panel*) to the medium of wild type cells and cav-1-KO cells. To control whether the tagged fluorophore supports peptide internalization, the uptake of TAMRA* alone at the same concentration as the peptides was studied (Fig. 3*C*, *bottom panel*). For each experiment confocal optical sections are displayed at high and low magnification. Because of the large size of these cells, it was not possible to show a higher number of cells per field and at the same time keep imaging parameters constant throughout all experiments. No difference of TAT transduction between WT and cav-1-KO cells was found. TAT also became internalized by an endocytic route, as indicated by the punctated intracellular fluorescence. This signal was still present in the caveolin-deficient cells. In contrast to TAT, the PTD_4 peptide entered the cells only by the endocytic mode and could not be detected freely inside the cyto- and nucleoplasm and the nucleolus (Fig. 3*C*, *middle panel, arrow-*

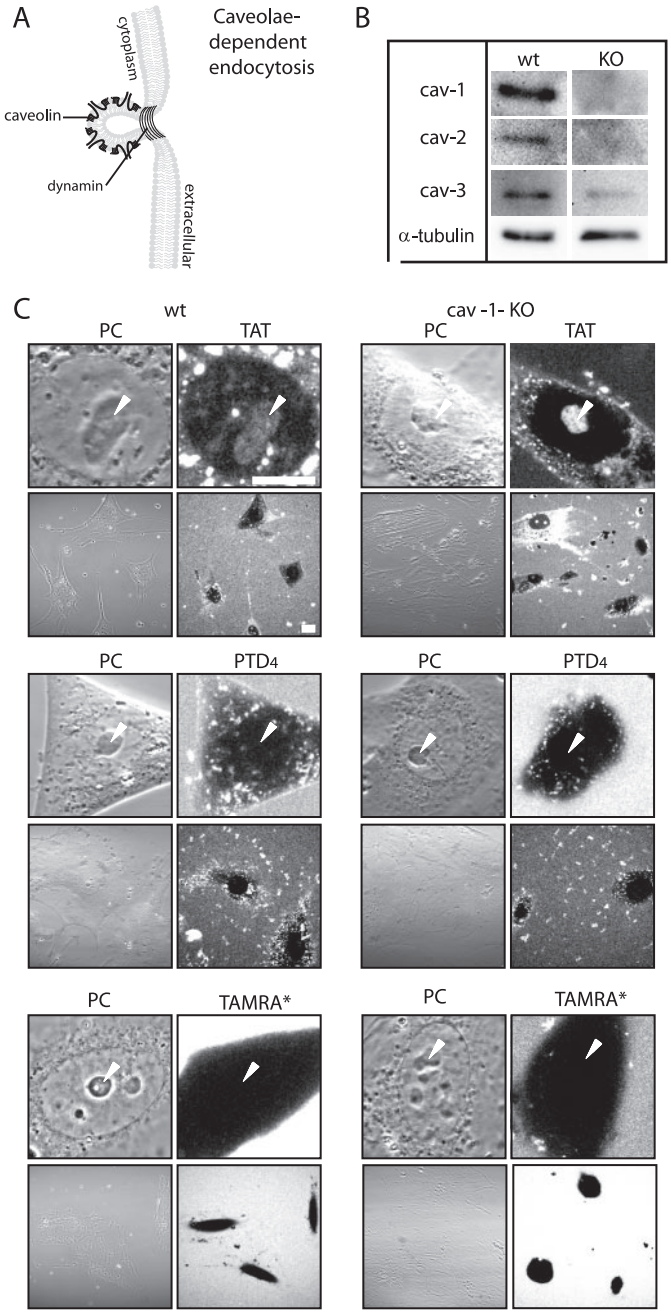

FIGURE 3. **Transduction of TAT is independent of caveolin-mediated endocytosis.** *A,* schematic diagram illustrating structural features of flask-shaped caveolae, which are lined by caveolin. Caveolae-mediated endocytosis is driven by a coat made of the integral membrane proteins caveolin-1, -2, or -3. Dynamin is required for the scission of caveolae. *B,* Western blot analysis of the integral membrane proteins caveolin (cav) -1, -2, and -3 in WT and caveolin 1 KO endothelioma cells. α-Tubulin is used to control for loading. *C,* confocal optical sections of living cells during incubation with the fluorescent CPPs TAT (*upper panel*) or PTD_4 (*mid panel*) and the fluorophore TAMRA* (*bottom panel*). Each panel displays images of the phase contrast (*PC*) and the peptide or fluorophore fluorescence at high magnification to display their intracellular distribution and at low magnification to highlight the frequency of CPP transduction in WT and cav-1-KO cells (see also supplemental Fig. S4). Whereas the amphipathic control peptide PTD_4 and the fluorophore TAMRA* were not transduced, the CPP TAT was homogeneously distributed in the cytoplasm, and it reached the nucleus where it accumulated inside the nucleolar compartment (marked by *arrowheads*). Both CPPs displayed vesicular uptake in WT and cav-1-KO cells. *Scale bar,* 10 μm for high and 20 μm for low magnification images.

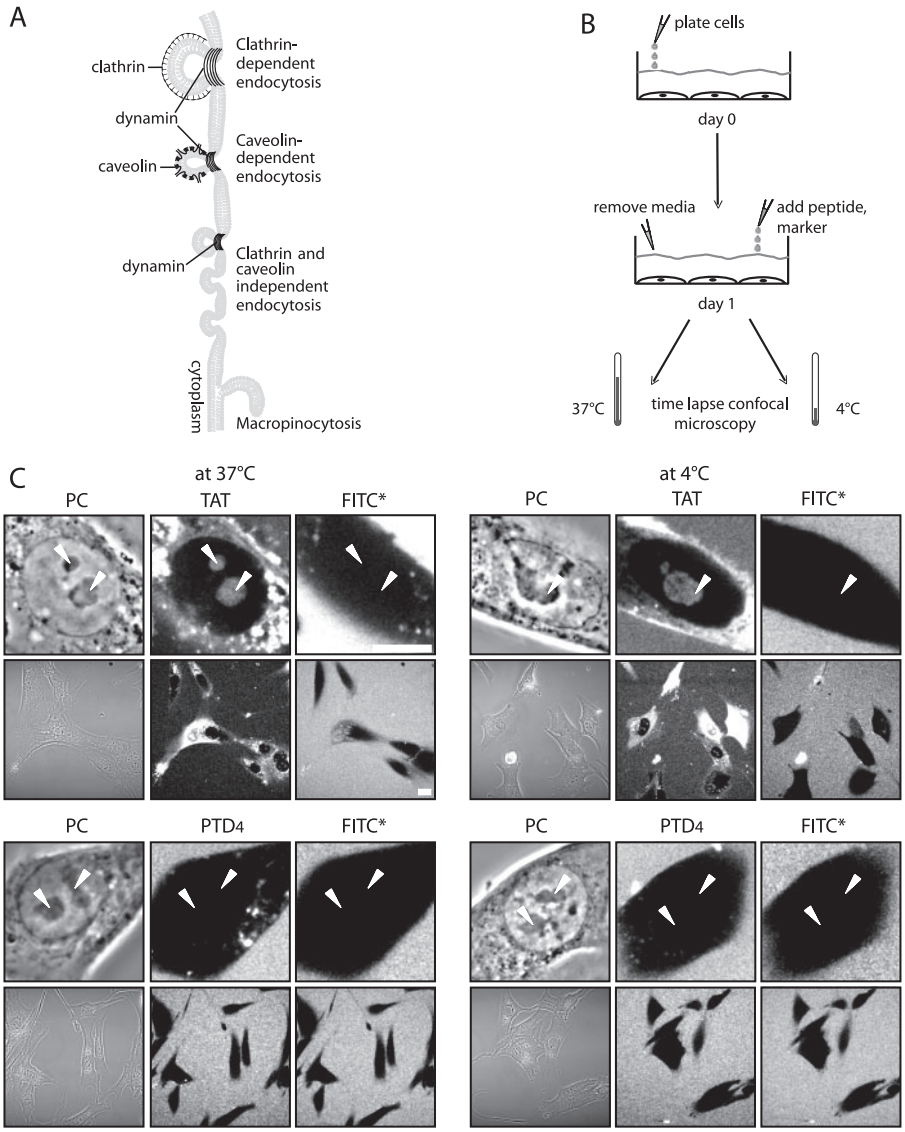

FIGURE 4. **Transduction of TAT is independent of endocytosis.** *A,* schematic overview of the different pathways of endocytic internalization that are suppressed at 4 °C: clathrin- and caveolin-dependent endocytosis, clathrin- and caveolin-independent endocytosis, and macropinocytosis. *B,* experimental strategy for transduction experiments performed at 37 and 4 °C. *C,* confocal optical sections of living cells during incubation with the fluorescent CPPs TAT (*upper panel*) or PTD_4 (*lower panel*) in the presence of the fluorophore FITC* as a small molecule marker to control for membrane pores or damage. Each panel displays high magnification images of the phase contrast (*PC*) and the fluorescently labeled peptide or fluorophore to show their uptake and intracellular distribution and low magnification images to highlight the frequency of transduction at 37 and 4 °C (see also supplemental Fig. S5). *Arrowheads* mark the position of nucleoli. The transduction experiments were performed in BHK21 cells kept at 37 and 4 °C. Although no intracellular vesicles were found at 4 °C, the transduction of TAT (nonvesicular, diffuse fluorescence with accumulation inside nucleoli) remained unchanged both at 37 and 4 °C. In contrast, the amphipathic control peptide PTD_4 and fluorophore FITC* were not transduced at 37 °C nor at 4 °C. *Scale bars* are 10 μm for high and 20 μm for low magnification images.

heads). TAMRA was excluded from the cytoplasm and intracellular compartments providing strong evidence that peptide uptake is not aided by the fluorophore. Based on these results, we conclude that caveolae-mediated endocytosis is not involved in the uptake mode of transduction of TAT conjugated to an LMW cargo.

Uptake of CPPs upon Shutting Off Endocytic Pathways—Because neither clathrin- nor caveolin-dependent endocytosis inhibits CPP uptake and in both cases we could still find TAT-containing vesicles concomitantly with freely available cytoplasmic TAT peptide, we tried next to inhibit all endocytic pathways simultaneously.

For this purpose, we followed the internalization of TAT and PTD_4 at low temperature, 4 °C. Fig. 4*A* depicts all potential endocytic uptake routes in cells that are expected to be inhibited under such conditions. Previous reports addressing the uptake of arginine-rich CPPs with LMW cargos into living cells are inconsistent. Although some reports insisted on the inability of CPPs to penetrate cells at low temperature and hence endocytosis would be required for internalization (49), according to other reports, CPP uptake is not inhibited at 4 °C (14, 19, 20). Fig. 4*B* displays the experimental setup for assessing the transduction ability of TAT and PTD_4 in C2C12 mouse myoblasts (data not shown) and in BHK21 hamster fibroblasts in the presence (37 °C) and absence (4 °C) of endocytosis by time-lapse confocal microscopy. To make sure that potential membrane lesions generated by low temperature conditions would not corrupt the transduction assay, the fluorophore FITC* was applied simultaneously with the TAMRA-labeled peptides to the cells. In case of severe membrane damage or pore formation induced by the peptides, the 389-Da-sized FITC* molecule should also be detectable intracellularly. Our observations displayed as high and low magnification images in Fig. 4*C* and supplemental Fig. S5 reveal that even at 4 °C TAT entered living cells and distributed over the cytoplasm and nucleus, where it accumulated inside nucleoli. At the same time the fluorophore FITC* did not gain access to intracellular compartments indicating that the plasma membrane was not compromised. The complete obstruction of endocytosis was further confirmed by the absence of fluorescently labeled vesicles at 4 °C. Vesicles were not observed for the CPP TAT nor for PTD_4. Furthermore, uptake of the globular TAT fusion protein TAT-bt-SAv that is restricted to endocytosis (8) was also blocked on the level of the plasma membrane at 4 °C (supplemental Fig. S2). These results prove unambiguously that arginine-rich CPPs like TAT are capable of reaching intracellular compartments of living cells by a mechanism that is independent of

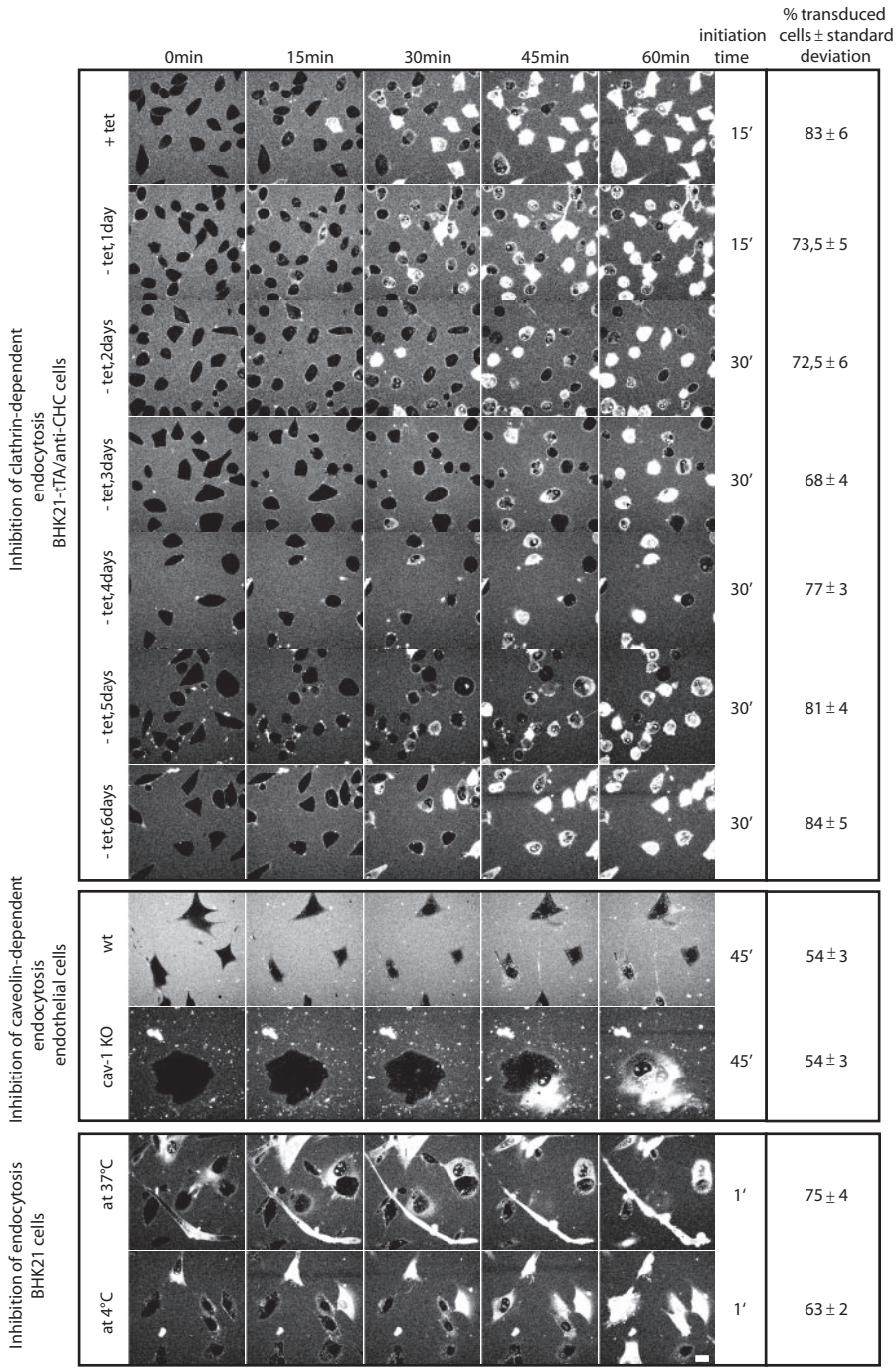

FIGURE 5. **Kinetic and quantitative analysis of transduction.** Assembly of confocal optical sections of living cells with time intervals of 15 min derived from the 60-min time lapses (see supplemental movies S1–S10) displaying the kinetics of TAT uptake in the different cell lines. All cell lines showed an unchanged transduction behavior in the control cells and the cells that were inhibited for a distinct or all pinocytic events. But the average entry time point of the TAT peptide is cell type-specific. The *last column* summarizes the transduction frequencies of TAT after 60 min of incubation in cells, where distinct or all endocytic pathways were suppressed. Transduction frequency was scored by counting the percentage of cells showing the intracellular freely available peptide (see Fig. 1, *B* and *C*). *Scale bar,* 10 μm.

endocytosis. However, the data also clearly show that a minimal number of arginines is crucial to permit transduction.

Frequency and Initiation Time of TAT Transduction—To quantify our results on the transduction ability in the absence of a distinct pathway or all pathways of endocytosis, we evaluated the percentages of transduced cells after 60 min of incubation with the CPP TAT and the initiation time of transduction (Fig. 5 and supplemental movies S1–S10). The control cells (+tet, day 0) showed a transduction frequency of 83%. While over the first 3 days after induction of the conditional knockdown of CHC (−tet) the transduction percentages were reduced to 68%, they recovered back to 84% transduction frequencies by day 6, although the internalization of fluorescently labeled transferrin was reduced by 90%. The frequency of transduced cells was identical in cav-1-deficient and isogenic WT cells (54%), although in these cells it was lower than in the BHK21-tTA/anti-CHC cells. Finally, the inhibition of all potential pinocytic pathways at 4 °C determined in BHK21 fibroblasts revealed that the transduction of the TAT peptide is diminished about 12% in comparison with transduction occurring in cells kept at 37 °C, but still 63% of the cells displayed nucleolar accumulation of TAT.

In BHK21-tTA/anti-CHC cells, the transduction mode of uptake initiated between 15 and 30 min of peptide addition after CHC knockdown as well as in control cells. The kinetics of peptide uptake in cav-1-KO and wild type cells displayed an uptake initiation at 45 min after application of TAT. The fastest uptake of TAT occurred in BHK21 fibroblasts within 1 min of addition to the medium and independent of temperature. A summary of the uptake kinetics of TAT peptide in all conditions tested is presented in Fig. 5.

In conclusion, the frequency and initiation time of TAT transduction was unchanged within a given cell type independent of endocytosis. However, both parameters were cell type-specific, suggesting that the membrane composition influences the velocity of transduction.

DISCUSSION

Despite the controversy and uncertainty regarding the uptake mechanism, the property of CPPs to deliver nonpermeable molecules into living cells makes them attractive vectors to

be used in biological sciences as well as in medicine and biotechnology. Former studies used chemical inhibitors of endocytosis to assign the uptake of CPPs to a particular endocytic pathway. However, the potential side effects and lack of specificity of such inhibitors make these studies difficult to interpret. Either the chemical compounds affect more than one specific pathway, like methyl-β-cyclodextrin that affects both lipid raft (26) and caveolin-coated vesicle formation (50) hence also caveolin-dependent endocytosis, or they have other side effects that may impact the import of RRPs, *e.g.* chlorpromazine was shown to interface with a number of Ca^{2+}-dependent signaling pathways (51) and to bind to dopamine receptors (19, 52). Thus, we have used genetically modified systems or physical methods to clarify the role of endocytosis in the translocation of RRPs.

The different phenotypes shown in Fig. 1 permit at least two explanations for the occurrence of free RRPs inside the cytoplasm and nucleoplasm. Either RRPs become endocytosed and a portion of the peptide stored in vesicles gets released into the cytoplasm or a second nonendocytic entry route that allows RRPs to directly cross the plasma membrane has to be considered.

Earlier reports associated uptake of RRPs with and without attached cargos to distinct endocytic pathways (16, 23–28, 39, 40, 49). However, our results unambiguously demonstrate that the transduction of TAT into living cells is not dependent on any endocytic or pinocytic events. We could exclude the pathway of clathrin-mediated endocytosis by a carefully controlled knockdown experiment. Also caveolin-mediated endocytosis was not involved in TAT translocation, because caveolin knock-out cells showed an identical transduction frequency to the wild type cells. Most importantly, TAT was not excluded from cells that were gently transferred to 4 °C, a state where all potential endocytic pathways are inhibited.

It is noteworthy to mention that the amount of TAT transduced into a cell varies between cells within a single experiment, but its intracellular distribution does not. This phenomenon was observed in every cell type and was independent of which endocytic route was down-regulated. (Fig. 2–5 and supplemental Fig. S3–S5).

Comparing the transduction frequencies of the specific cell types, a variation from 68 to 84% for the BHK21-tTA/anti-CHC cell line, over 63–75% in BHK21 cells, and to 54% in the mouse endothelioma cells can be found, suggesting that the particular membrane composition of different cell types impacted on transduction (Fig. 5). This was further corroborated by the observation that the average initiation time of transduction was cell type-specific, but it did not change upon the inhibition of endocytosis within a given cell type. All experiments were conducted in addition to PTD_4 as a representative CPP (29) with a reduced number of arginines compared with TAT. At the same concentration, this peptide did not gain access to the intracellular compartments in a freely diffusing form and was internalized exclusively by endocytosis. This could be explained by the fact that a minimal number of six arginines is required to permit transduction (18). Instead, PTD_4 was predominantly internalized by the clathrin-dependent pathway. Although not capable of performing transduction, the CPP PTD_4 was endocytosed more efficiently than non-CPP compounds added to the medium, *e.g.* the fluorophore TAMRA* alone (Fig. 3*C*).

Recent mechanistic studies with artificial membrane systems described the formation of pores as a consequence of the interaction with intermediate concentrations of the RRP TAT (53). However, the fluorophore FITC*, concomitantly applied to the cells together with the TAT peptide, remained outside of the cells, whereas TAT transduced selectively into the cells (Fig. 4*C*), arguing against the formation of nonselective pores.

In summary, our data indicate that TAT CPP internalization is independent of endocytosis and occurs without disruption of the cell membrane. These properties and its high intracellular bioavailability make TAT CPP a very effective tool to deliver small compounds into living cells.

Acknowledgments—We thank Kirsten Sandvig for the generous gift of the BHK-tTA/anti-CHC cell line. We are indebted to our colleagues Petra Domaing for help in the cell culture, Robert Martin and Jeff Stear for fruitful discussions and support with microscopy, and Sebastian Haase for advice in the image analysis.

REFERENCES

1. Frankel, A. D., and Pabo, C. O. (1988) *Cell* **55,** 1189–1193
2. Green, M., and Loewenstein, P. M. (1988) *Cell* **55,** 1179–1188
3. Dietz, G. P., and Bahr, M. (2007) *Methods Mol. Biol.* **399,** 181–198
4. Nori, A., Jensen, K. D., Tijerina, M., Kopeckova, P., and Kopecek, J. (2003) *Bioconjugate Chem.* **14,** 44–50
5. Mann, D. A., and Frankel, A. D. (1991) *EMBO J.* **10,** 1733–1739
6. Shibagaki, N., and Udey, M. C. (2002) *J. Immunol.* **168,** 2393–2401
7. Tunnemann, G., Karczewski, P., Haase, H., Cardoso, M. C., and Morano, I. (2007) *J. Mol. Med.* **85,** 1405–1412
8. Tunnemann, G., Martin, R. M., Haupt, S., Patsch, C., Edenhofer, F., and Cardoso, M. C. (2006) *FASEB J.* **20,** 1775–1784
9. Astriab-Fisher, A., Sergueev, D., Fisher, M., Shaw, B. R., and Juliano, R. L. (2002) *Pharmacol. Res.* **19,** 744–754
10. Fawell, S., Seery, J., Daikh, Y., Moore, C., Chen, L. L., Pepinsky, B., and Barsoum, J. (1994) *Proc. Natl. Acad. Sci. U. S. A.* **91,** 664–668
11. Nagahara, H., Vocero-Akbani, A. M., Snyder, E. L., Ho, A., Latham, D. G., Lissy, N. A., Becker-Hapak, M., Ezhevsky, S. A., and Dowdy, S. F. (1998) *Nat. Med.* **4,** 1449–1452
12. Schwarze, S. R., Ho, A., Vocero-Akbani, A., and Dowdy, S. F. (1999) *Science* **285,** 1569–1572
13. Lewin, M., Carlesso, N., Tung, C. H., Tang, X. W., Cory, D., Scadden, D. T., and Weissleder, R. (2000) *Nat. Biotechnol.* **18,** 410–414
14. Iwasa, A., Akita, H., Khalil, I., Kogure, K., Futaki, S., and Harashima, H. (2006) *Biochim. Biophys. Acta* **1758,** 713–720
15. Torchilin, V. P., Rammohan, R., Weissig, V., and Levchenko, T. S. (2001) *Proc. Natl. Acad. Sci. U. S. A.* **98,** 8786–8791
16. Drin, G., Cottin, S., Blanc, E., Rees, A. R., and Temsamani, J. (2003) *J. Biol. Chem.* **278,** 31192–31201
17. Richard, J. P., Melikov, K., Vives, E., Ramos, C., Verbeure, B., Gait, M. J., Chernomordik, L. V., and Lebleu, B. (2003) *J. Biol. Chem.* **278,** 585–590
18. Tunnemann, G., Ter-Avetisyan, G., Martin, R. M., Stockl, M., Herrmann, A., and Cardoso, M. C. (2008) *J. Pept. Sci.* **14,** 469–476
19. Duchardt, F., Fotin-Mleczek, M., Schwarz, H., Fischer, R., and Brock, R. (2007) *Traffic* **8,** 848–866
20. Fretz, M. M., Penning, N. A., Al-Taei, S., Futaki, S., Takeuchi, T., Nakase, I., Storm, G., and Jones, A. T. (2007) *Biochem. J.* **403,** 335–342
21. Ziegler, A., Nervi, P., Durrenberger, M., and Seelig, J. (2005) *Biochemistry* **44,** 138–148
22. Mayor, S., and Pagano, R. E. (2007) *Nat. Rev. Mol. Cell Biol.* **8,** 603–612
23. Richard, J. P., Melikov, K., Brooks, H., Prevot, P., Lebleu, B., and Chernomordik, L. V. (2005) *J. Biol. Chem.* **280,** 15300–15306
24. Ferrari, A., Pellegrini, V., Arcangeli, C., Fittipaldi, A., Giacca, M., and Bel-

tram, F. (2003) *Mol. Ther.* **8,** 284–294
25. Fittipaldi, A., Ferrari, A., Zoppe, M., Arcangeli, C., Pellegrini, V., Beltram, F., and Giacca, M. (2003) *J. Biol. Chem.* **278,** 34141–34149
26. Kaplan, I. M., Wadia, J. S., and Dowdy, S. F. (2005) *J. Controlled Release* **102,** 247–253
27. Nakase, I., Tadokoro, A., Kawabata, N., Takeuchi, T., Katoh, H., Hiramoto, K., Negishi, M., Nomizu, M., Sugiura, Y., and Futaki, S. (2007) *Biochemistry* **46,** 492–501
28. Wadia, J. S., Stan, R. V., and Dowdy, S. F. (2004) *Nat. Med.* **10,** 310–315
29. Ho, A., Schwarze, S. R., Mermelstein, S. J., Waksman, G., and Dowdy, S. F. (2001) *Cancer Res.* **61,** 474–477
30. Iversen, T. G., Skretting, G., van Deurs, B., and Sandvig, K. (2003) *Proc. Natl. Acad. Sci. U. S. A.* **100,** 5175–5180
31. Drab, M., Verkade, P., Elger, M., Kasper, M., Lohn, M., Lauterbach, B., Menne, J., Lindschau, C., Mende, F., Luft, F. C., Schedl, A., Haller, H., and Kurzchalia, T. V. (2001) *Science* **293,** 2449–2452
32. Yaffe, D., and Saxel, O. (1977) *Nature* **270,** 725–727
33. Futaki, S., Suzuki, T., Ohashi, W., Yagami, T., Tanaka, S., Ueda, K., and Sugiura, Y. (2001) *J. Biol. Chem.* **276,** 5836–5840
34. Rothbard, J. B., Kreider, E., VanDeusen, C. L., Wright, L., Wylie, B. L., and Wender, P. A. (2002) *J. Med. Chem.* **45,** 3612–3618
35. Suzuki, T., Futaki, S., Niwa, M., Tanaka, S., Ueda, K., and Sugiura, Y. (2002) *J. Biol. Chem.* **277,** 2437–2443
36. Marsh, M., and Helenius, A. (2006) *Cell* **124,** 729–740
37. Nitschke, M., Korte, T., Tielesch, C., Ter-Avetisyan, G., Tunnemann, G., Cardoso, M. C., Veit, M., and Herrmann, A. (2008) *Virology* **377,** 248–254
38. Martin-Acebes, M. A., Gonzalez-Magaldi, M., Sandvig, K., Sobrino, F., and Armas-Portela, R. (2007) *Virology* **369,** 105–118
39. Kawamura, K. S., Sung, M., Bolewska-Pedyczak, E., and Gariepy, J. (2006) *Biochemistry* **45,** 1116–1127
40. Vendeville, A., Rayne, F., Bonhoure, A., Bettache, N., Montcourrier, P., and Beaumelle, B. (2004) *Mol. Biol. Cell* **15,** 2347–2360
41. Gossen, M., and Bujard, H. (1992) *Proc. Natl. Acad. Sci. U. S. A.* **89,** 5547–5551
42. Bennett, E. M., Lin, S. X., Towler, M. C., Maxfield, F. R., and Brodsky, F. M. (2001) *Mol. Biol. Cell* **12,** 2790–2799
43. Feng, Y., Press, B., and Wandinger-Ness, A. (1995) *J. Cell Biol.* **131,** 1435–1452
44. Press, B., Feng, Y., Hoflack, B., and Wandinger-Ness, A. (1998) *J. Cell Biol.* **140,** 1075–1089
45. Soldati, T., and Schliwa, M. (2006) *Nat. Rev. Mol. Cell Biol.* **7,** 897–908
46. Anderson, R. G. (1998) *Annu. Rev. Biochem.* **67,** 199–225
47. Simons, K., and Ikonen, E. (1997) *Nature* **387,** 569–572
48. Torgersen, M. L., Skretting, G., van Deurs, B., and Sandvig, K. (2001) *J. Cell Sci.* **114,** 3737–3747
49. Zorko, M., and Langel, U. (2005) *Adv. Drug Delivery Rev.* **57,** 529–545
50. Saalik, P., Elmquist, A., Hansen, M., Padari, K., Saar, K., Viht, K., Langel, U., and Pooga, M. (2004) *Bioconjugate Chem.* **15,** 1246–1253
51. Marshak, D. R., Lukas, T. J., and Watterson, D. M. (1985) *Biochemistry* **24,** 144–150
52. Seeman, P. (2002) *Can. J. Psychiatry* **47,** 27–38
53. Herce, H. D., and Garcia, A. E. (2007) *Proc. Natl. Acad. Sci. U. S. A.* **104,** 20805–20810

SUPPLEMENTARY FIGURES

Figure S1

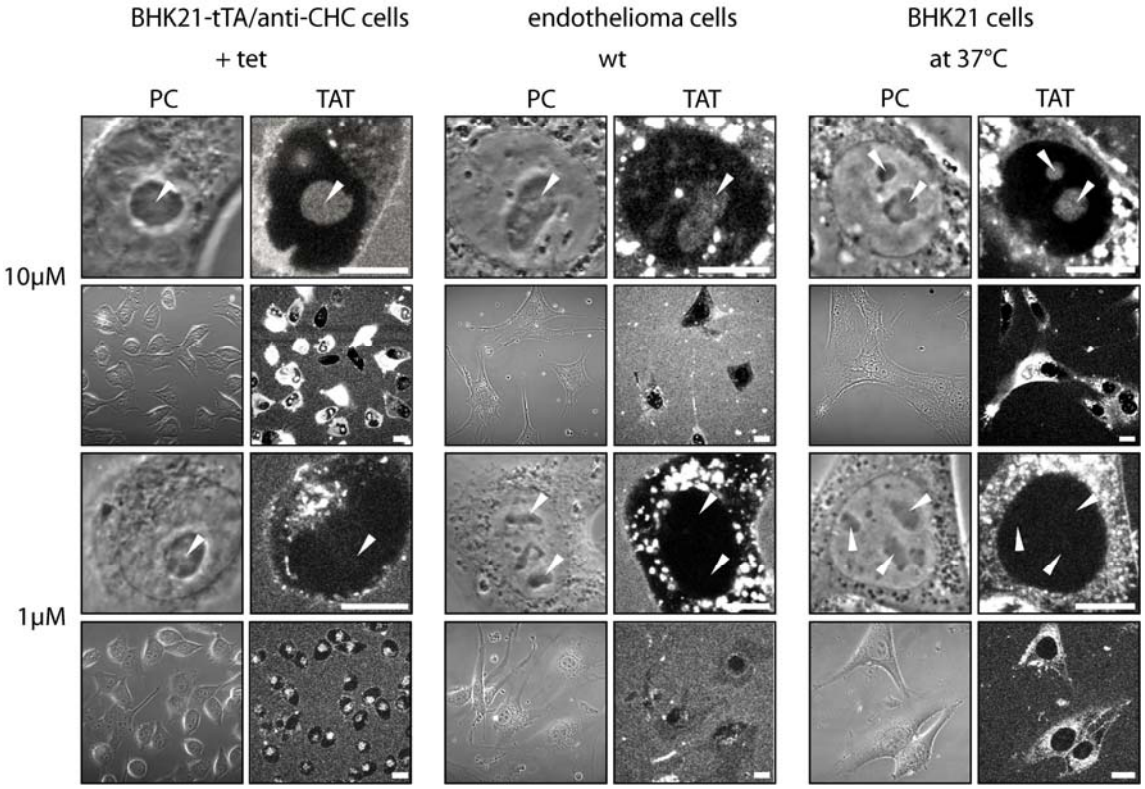

Fig. S1. Concentration-dependent mode of uptake of TAT CPP. TAT was incubated with the cells indicated at 1 and 10 µM concentration for one hour. Confocal optical sections of living cells are displayed with phase contrast (PC) and fluorescence images to show the uptake mode and intracellular distribution of TAT. Each panel contains high and low magnification images. Below a certain threshold concentration, transduction of TAT CPP, (visualized by the presence of peptide freely available in the cytoplasm and accumulation in the nucleolus (arrowheads) as shown in Fig. 1-5) does not occur whereas endocytosis of the TAT CPP persists as shown here. Scale bar 10µm for high and 20 µm for low magnification images.

Figure S2

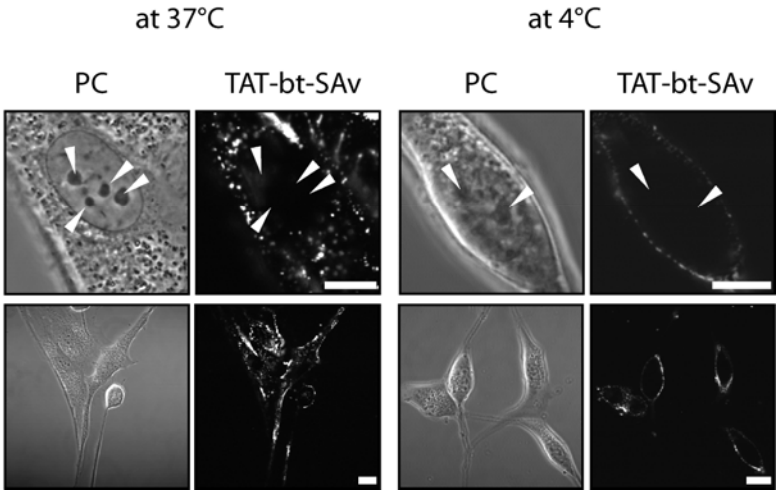

Fig. S2. Low temperature incubation abrogates all endocytic pathways. Mouse fibroblasts were incubated at 37°C and 4° C with the globular protein TAT-biotin-streptavidin-Cy5 (TAT-bt-SAv) as an additional fluid phase marker to the peptide PTD_4 and the fluorophore FITC* shown in Fig. 4. Confocal optical sections of living cells are shown as high and low magnifications after one hour incubation with the globular TAT-fusion protein. Arrowheads mark the nucleoli. Protein uptake was blocked at the level of the plasma membrane at a temperature of 4°C, whereas at 37°C the protein became rapidly internalized into vesicles. Scale bar 10µm for high and 20 µm for low magnification images.

Figure S3

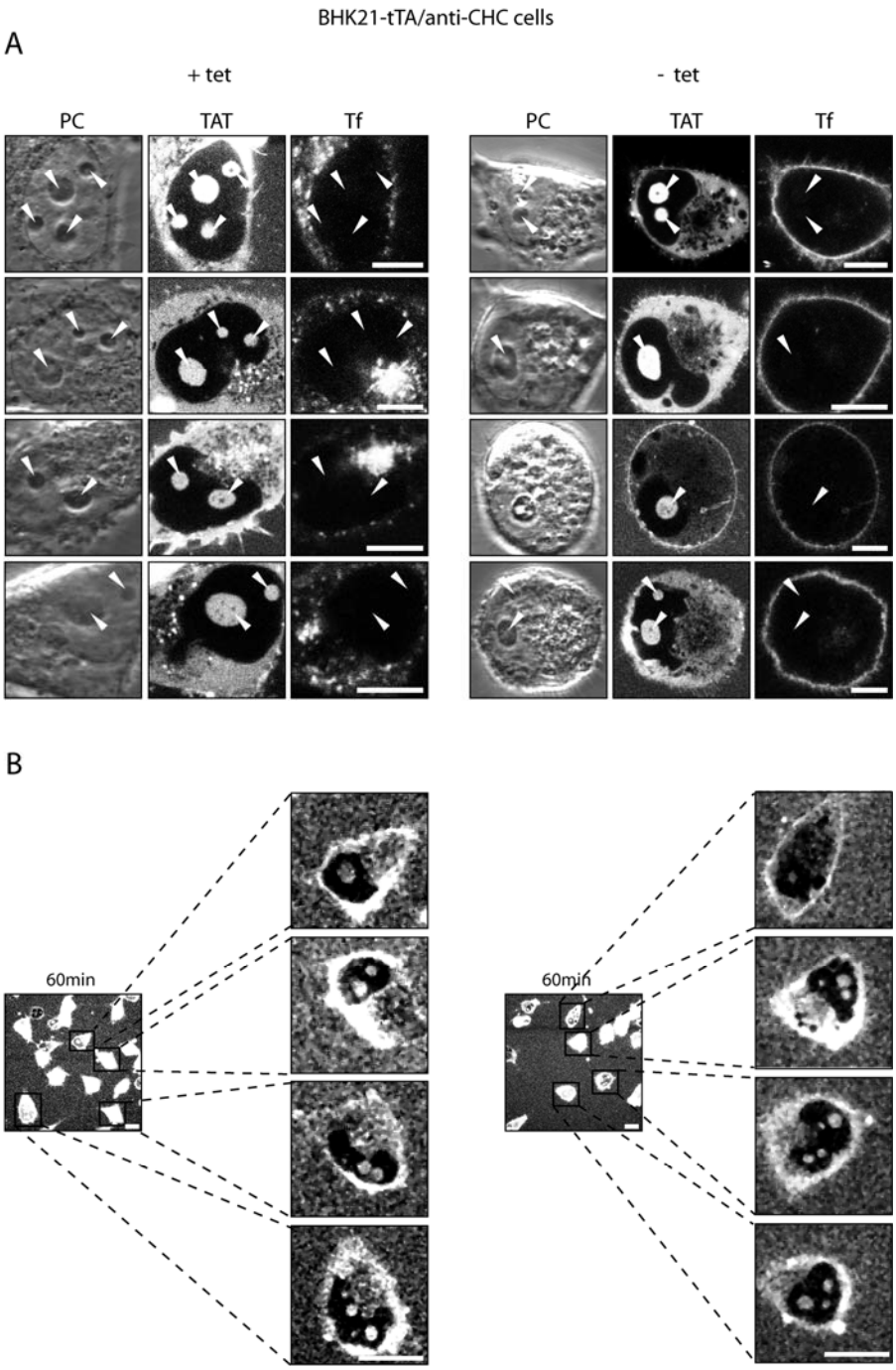

Fig. S3. Transduction of TAT is independent of clathrin-mediated endocytosis. Additional examples to the ones depicted in Fig. 2 are shown as high magnification images (*A*) and images magnified from the online supplementary movies S1 and S7 (*B*) after incubation with the TAT peptide for 60 minutes. Confocal optical sections of living cells during incubation with the fluorescent CPP TAT in the presence of transferrin (Tf) as a marker for clathrin-dependent endocytosis (only *A*). The control cells (left panel) and the cells after knockdown of the clathrin heavy chain (right panel) are shown as images of the phase contrast (PC) and the peptide (*A*) or of the peptide alone (*B)*. Arrowheads mark the position of nucleoli (*A*). While uptake of Tf is nearly abolished after tetracycline removal over a period of six days (*A*) and vesicular uptake of TAT is reduced, the TAT CPP is still capable of reaching all intracellular compartments (non-vesicular, cytoplasmic and nucleolar fluorescence), indicating that this mode of uptake is not influenced by clathrin-dependent endocytosis. Scale bar 10 μm.

Figure S4

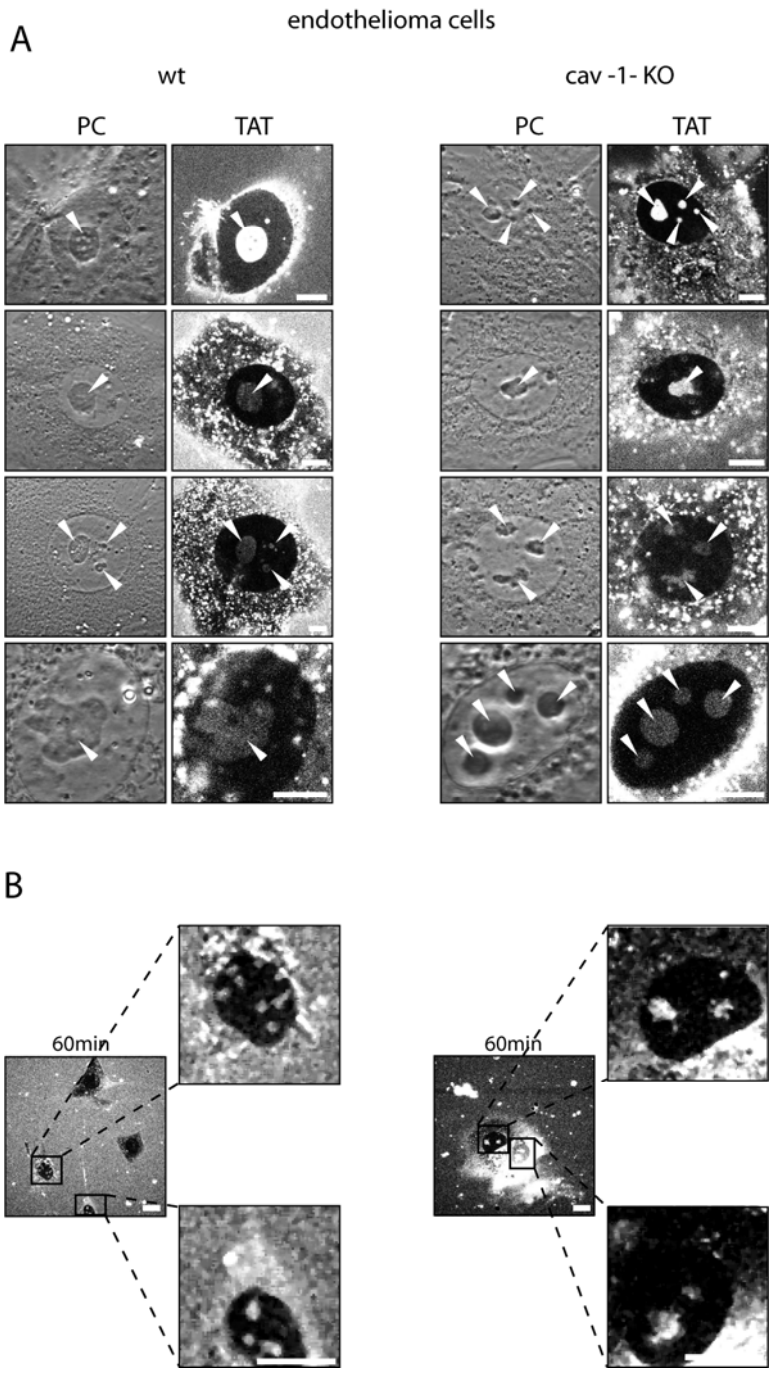

Fig. S4. Transduction of TAT is independent of caveolin-mediated endocytosis. Additional examples to the ones depicted in Fig. 3 are shown as high magnification images (*A*) and images magnified from the online supplementary movies S8 and S9 (*B)* after incubation with the TAT peptide for 60 minutes. Confocal optical sections of the wild type (left panel, wt) and caveolin-1 knockout (right panel, cav-1-KO) cells during incubation with the fluorescent CPP TAT. *A*-panels display images of the phase contrast (PC) and the peptide, *B*-panels only the peptide fluorescence images. Neither vesicular uptake of the CPP TAT nor the amount of TAT that was homogeneously distributed in the cytoplasm and accumulated inside the nucleolar compartment (marked by arrowheads), was different in both cases. Scale bar 10 μm.

Figure S5

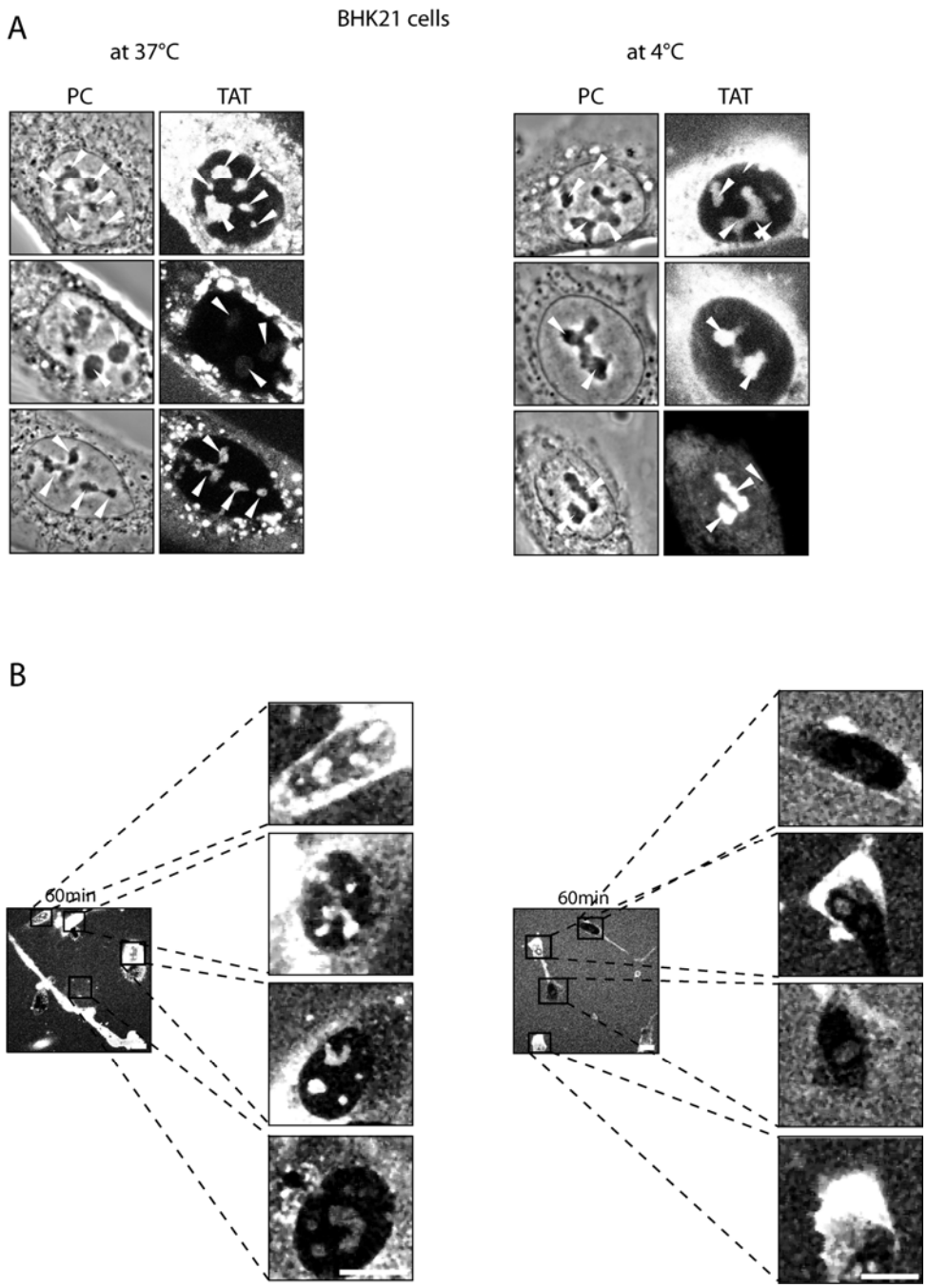

Fig. S5. Transduction of TAT is independent of endocytosis. Additional examples to the ones depicted in Fig. 4 are shown as high magnification images (*A*) and images magnified from the online supplementary movie S10 (*B)* after incubation with the TAT peptide for 60 minutes at 37°C (left panel) and at 4°C (right panel). In *A* each panel displays the phase contrast (PC) and the fluorescently labelled peptide. Arrowheads mark the position of nucleoli as unambiguous sign of freely diffusing intracellular TAT. In *B* the fluorescence of the labelled TAT-peptide is displayed. The transduction experiments were performed in BHK21 cells kept at the indicated temperatures before and during the experiment. Whereas there was no vesicle formation at 4°C (*A*) the transduction of TAT remained unchanged both at 37°C and 4°C (*A* and *B*). Scale bar 10 µm.